Signals of the QCD phase transition in core collapse supernovae—microphysical input and implications on the supernova dynamics

2010 Class. Quantum Grav. 27 114102

(http://iopscience.iop.org/0264-9381/27/11/114102)

IOP PUBLISHING CLASSICAL AND QUANTUM GRAVITY

Class. Quantum Grav. **27** (2010) 114102 (11pp) doi:10.1088/0264-9381/27/11/114102

Signals of the QCD phase transition in core collapse supernovae—microphysical input and implications on the supernova dynamics

T Fischer[1], I Sagert[2], M Hempel[3], G Pagliara[3], J Schaffner-Bielich[3] and M Liebendörfer[1]

[1] Department of Physics, University of Basel, Klingelbergstrasse 82, 4056 Basel, Switzerland
[2] Institut für Theoretische Physik, Goethe-Universität, Max-von-Laue-Str. 1, 60438 Frankfurt Germany
[3] Institut für Theoretische Physik, Ruprecht-Karls-Universität, Philosophenweg 16, 69120 Heidelberg, Germany

Received 10 December 2009, in final form 20 January 2010
Published 10 May 2010
Online at stacks.iop.org/CQG/27/114102

Abstract

In contrast to heavy ion collisions, matter in astrophysical systems such as neutron stars, compact star mergers and supernova environments can be highly isospin asymmetric. We focus on core collapse supernova matter where temperatures reach tens of MeV. Both conditions, the high temperatures and isospin asymmetry, can favour an early phase transition to quark matter already close to nuclear saturation density. We examine the QCD phase transition during the early postbounce phase of core collapse supernovae. We discuss the microphysical input, i.e. the modelling of the phase transition to strange quark matter, and the consequences on the dynamical evolution as well as the observable neutrino signal from the phase transition. The equation of state for strange quark matter is based on the MIT bag model. The phase transition is constructed applying the Gibbs criterion which results in an extended coexistence region in the phase diagram between the hadronic and the quark phases, i.e. the mixed phase. The supernovae are simulated via general relativistic radiation hydrodynamics based on three-flavour Boltzmann neutrino transport in spherical symmetry. The dynamical evolution of the phase transition to quark matter is determined by an adiabatic collapse due to the softening of the equation of state in the mixed phase. The equation of state for the pure quark phase stiffens again which causes the collapse to halt and a shock wave forms at the boundary between the mixed and the pure hadronic phases. This shock accelerates and launches an explosion, which releases a burst of neutrinos dominated by electron anti-neutrinos due to the lifted degeneracy of the shock-heated hadronic material.

PACS numbers: 21.65.Cd, 21.65.Mn, 21.65.Qr, 23.40.Bw, 25.75.Nq, 26.30.Jk, 26.50.+x, 47.35.−i, 47.75.+f, 97.60.Bw, 97.60.Lf

1. Introduction

Stars more massive than 8 $M_\odot$ develop extended Fe-cores at the end of stellar evolution. Since Fe-group nuclei are the most stable elements with the smallest binding energy per nucleon, the nuclear burning processes stop. Weak reactions, in particular electron captures on nuclei, become important. The emitted electron neutrinos can escape because matter inside stellar cores at the end of stellar evolution corresponds to the neutrino free-streaming regime. The loss of lepton number, in combination with the photodisintegration of heavy nuclei, causes the Fe-core to contract. The contraction proceeds into a collapse during which the central density and temperature increase. Due to the repulsive nuclear interaction around saturation density, the collapse halts and the Fe-core bounces back. This results in an outward propagating dynamic shock wave accompanied by matter outflow. However, heavy nuclei fall continuously onto the shock and dissociate into light nuclei and free nucleons. Furthermore, as soon as the expanding shock wave propagates across the neutrinospheres, i.e. the neutrino energy and flavour-dependent spheres of last scattering, additional electron captures release a burst of electron neutrinos. These neutrinos carry away energy of several 10^{53} erg s^{-1} on a timescale of 10–20 ms after bounce. As a consequence of this energy loss in combination with the dissociation of infalling heavy nuclei, the expanding shock wave turns into a standing accretion shock (SAS) with no matter outflow already about 5 ms after bounce. A hot and lepton-rich central object forms immediately after bounce—the so-called protoneutron star (PNS). Its central density is of the order of nuclear saturation density, i.e. $\rho_0 \simeq 2 - 4 \times 10^{14}$ g cm^{-3}. Since the energy in the neutrino radiation field is of the order 10^{53} erg and kinetic explosion energies are of the order 10^{51} erg, the revival of the SAS and the consequent explosion have long been investigated via the deposition of neutrino energy, leading to neutrino-driven explosions [1]. Neutrinos are continuously emitted at high matter densities and transported outwards to lower densities where the neutrino absorption processes deposit a part of the radiation energy behind the oscillating SAS. However, neutrino-driven explosions in spherically symmetric models have only been obtained for the low mass 8.8 $M_\odot$ O-Ne-Mg-core [17–19], where the explosion is obtained on a short timescale of about 30 ms post bounce [6, 12]. The post bounce evolution of more massive Fe-core progenitors leads to an extended mass accretion phase during which the central PNS contracts on a timescale of 100 ms (depending on the mass accretion rate and the equation of state). The neutrino energy deposition becomes less efficient in spherically symmetric models, and neutrino heating fails to revive the SAS. Possible solutions have been found in multi-dimensional models where rotation and the development of convection have been shown to increase the neutrino heating efficiency [4, 9, 11, 15].

The evolution of the central PNS is essential for the neutrino spectra. On the other hand, one of the largest uncertainty in core collapse supernova models is the equation of state (EoS) for hot and dense nuclear matter. The regime of uncertainties corresponds to the thermodynamic properties found in PNS interiors, modelled as central object in core collapse simulations of massive stars. The thermodynamic state is given by temperatures of 5–50 MeV and central densities above nuclear saturation density ($\rho_{\rm central} \gtrsim \rho_0$). Matter is additionally isospin asymmetric with a low proton-to-baryon ratio, given by the electron fraction[4], of $Y_e \simeq 0.1$–0.3. These conditions favour the quark–hadron phase transition due to the relatively large symmetry energy of hadronic matter and the higher number of degrees of freedom in strange quark matter.

[4] In core collapse supernova simulations, the electron fraction Y_e equals the proton fraction Y_p due to charge neutrality and the absence of other charged particles such as μ or τ.

Neutron stars have long been studied as objects to probe the EoS for dense matter, also with respect to the presence of quark matter in their interiors. In the latter case, the neutron star is called a hybrid star if in addition to the quark core a hadronic envelope is present. Of special interest concerning the appearance of quark matter in astronomical events, and astrophysical processes are observable signals which could be related to the properties of the QCD phase transition. In the case of core collapse supernovae (SNe), gravitational waves (GWs) and the neutrinos emitted provide the only direct insights since these observables depend directly on the evolution inside stellar cores while dense matter is opaque for photons. Since GWs are difficult to detect, the most reliable information is due to the neutrino signal emitted. At present, although the only observed neutrino signal from a core collapse SN, i.e. SN1987A [2, 10], provided only very few data points, it nevertheless probed the predicted scenario to some extend. In order to calculate the neutrino lightcurve, detailed neutrino radiation hydrodynamics studies are required. The first attempt in this direction goes back to the late 1980s [21], where a relation to SN1987A was discussed. This study was based on a parametrized EoS and general relativistic hydrodynamics. A more sophisticated EoS and a treatment of deleptonization during the Fe-core collapse phase were included into the investigation of the quark–hadron phase transition where the critical conditions, i.e. the critical density ρ_c and temperature T_c for the appearance of quark matter, were obtained at core bounce of massive Fe-core progenitor stars [7]. The authors find the formation of a second shock wave as a direct consequence of the phase transition, which merges with the bounce shock shortly after. However, both studies could not predict the possible neutrino signal due to the lack of neutrino transport post bounce. More recently a sophisticated quark EoS based on the MIT bag model for the description of quark matter has been applied to core collapse simulations of very massive (100 $M_\odot$) progenitor stars [16]. Such stars will not explode but collapse to a black hole, where due to the softening of the EoS during the quark–hadron phase transition the time until black hole formation is shortened.

For the prediction of the neutrino spectra, accurate neutrino transport is required for the core collapse supernova evolution timescales of the order of several seconds. Additionally, the presence of strong gravitational fields and relativistic matter velocities close to the vacuum speed of light require the inclusion of general relativity for both hydrodynamics and radiation transport. These two aspects are beyond the present state-of-the-art multi-dimensional modelling of core collapse supernovae including spectral neutrino transport. We apply general relativistic radiation hydrodynamics in spherical symmetry based on three-flavour Boltzmann neutrino transport to simulations of low and intermediate mass Fe-core progenitors. The quark EoS constructed for this study is based on the MIT bag model, where the temperature and electron fraction-dependent critical density ρ_c is close to nuclear saturation density mainly due to the low electron fraction of supernova matter. The phase transition itself is constructed by applying the Gibbs conditions which results in an extended coexistence region between the hadron and quark phases in the phase diagram, i.e. the *mixed phase*.

The manuscript is organized as follows. In sections 2 and 3 we introduce our model including the quark matter description, followed by section 4 where the simulation results are discussed. We close with the summary in section 5.

2. General relativistic radiation hydrodynamics in spherical symmetry

The numerical model Agile–Boltztran applied to the present investigation of the QCD phase transition in core collapse supernovae is based on general relativistic radiation hydrodynamics

in spherical symmetry (for details, see [13] and references therein). The following line element describes non-stationary and spherically symmetric spacetime

$$\mathrm{d}s^2 = -\alpha^2\,\mathrm{d}t^2 + \left(\frac{r'}{\Gamma}\right)^2 \mathrm{d}a^2 + r(t,a)^2(\mathrm{d}\theta^2 + \sin^2\theta\ \mathrm{d}\phi^2), \tag{1}$$

where the spacetime coordinates are the coordinate time t, mass a and the two angles (θ, ϕ) which describe a 2-sphere of radius $r(t, a)$ and $r' = \partial r/\partial a$. The metric coefficient $\alpha(t, a)$ is the lapse function which determines time dilatation and $\Gamma(t, a) = \sqrt{1 - 2m/r + u^2}$, where $u = \partial r/\alpha\partial t$ is the matter velocity. The evolution equations are obtained by solving the conservation equations for energy and momentum $\nabla_i T^{ij} = 0$, i.e. the divergence of the stress–energy tensor

$$\begin{aligned} T^{tt} &= \rho(1 + e + J), \qquad T^{ta} = T^{at} = \rho H, \\ T^{aa} &= P + \rho K, \qquad T^{\theta\theta} = T^{\phi\phi} = p + \tfrac{1}{2}\rho(J - K), \end{aligned} \tag{2}$$

with the matter density ρ, internal energy density e and pressure p. Coupled to the hydrodynamic quantities is the neutrino radiation field where the additional contributions are the neutrino internal energy density J, the pressure K and the energy exchange between matter and radiation H. These quantities are the neutrino moments and are given by phase-space integration of the neutrino distribution function $f_\nu(t, a, \mu, E)$, where $\nu = (\nu_e, \bar{\nu}_e, \nu_{\mu/\tau}, \bar{\nu}_{\mu/\tau})$. In spherical symmetry, the neutrino distribution function depends on the spacetime coordinates as well as on the cosine of the propagation angle $\mu = \cos\theta$ and the neutrino energy E. The evolution of the distribution function, i.e. $\partial f/\alpha\partial t$, is obtained by solving the general relativistic Boltzmann transport equation for every neutrino flavour, where the neutrino trajectories are time-like geodesics in spacetime. A full description of the coupled radiation hydrodynamics equations can be found in [13]. In addition to the transport, neutrino interactions with matter contribute to the changes of the neutrino distribution function and must therefore be taken into account. It is referred to as the collision term of the Boltzmann equation. The following neutrino reactions are considered:

$$e^- + p \leftrightarrow n + \nu_e, \qquad e^+ + n \leftrightarrow p + \bar{\nu}_e, \qquad e^- + \langle A, Z\rangle \leftrightarrow \langle A, Z-1\rangle + \nu_e, \tag{3}$$

$$\nu + N \leftrightarrow \nu + N, \qquad \nu + \langle A, Z\rangle \leftrightarrow \nu + \langle A, Z\rangle, \qquad \nu + e^\pm \leftrightarrow \nu + e^\pm, \tag{4}$$

$$e^- + e^+ \leftrightarrow \nu + \bar{\nu}, \qquad N + N \leftrightarrow N + N + \nu + \bar{\nu}. \tag{5}$$

The electronic charged current reactions (3) are electron captures on free protons and nuclei with average atomic mass and charge $\langle A, Z\rangle$ as well as positron captures on free neutrons. Additionally neutral current reactions, such as scattering (4) and pair reactions (5), are taken into account. The calculation of the reaction rates is done iteratively following the standard Weinberg–Salam–Glashow theory (in first order) of weak interactions [3].

Neutrino flavour oscillations are not taken into account in the present study of the quark–hadron phase transition. Nevertheless, their impact on the neutrinos due to vacuum oscillations is important for the prediction of accurate spectra. Furthermore, the influence of MSW (Mikheyev, Smirnov, Wolfenstein) flavour conversions is important during the neutrino propagation through the stellar envelope. Both effects and the possible detectability of a galactic signal are studied in [5]. Collective flavour oscillations have been speculated to be of relevance for the neutrino propagation at higher densities, i.e. inside stellar cores. Their inclusion is difficult; it will couple the different flavour equations in the Boltzmann transport for the neutrino propagation. The implementation into our radiation hydrodynamics model is beyond the scope of the present paper.

The EoS in core collapse supernova simulations has to handle two intrinsically different thermodynamic regimes which can be separated by the temperature T as follows. (a) For $T < 0.5$ MeV, we apply an ideal gas approximation for the baryon contributions. In order to obtain the internal energy evolution, we use a nuclear reaction network [22] because time-dependent nuclear processes are important. (b) For $T \geqslant 0.5$ MeV, nuclei are in nuclear statistical equilibrium (NSE) where we use the baryon EoS based on the RMF approach and the Thomas–Fermi approximation [20]. It has a large compressibility of 281 MeV and symmetry energy of 36.9 MeV and results in a stiff EoS. Contributions from electrons and positrons as well as photons and ion–ion correlations (only for non-NSE) [23] are added for all temperatures.

3. The quark matter description

In this work, we consider additionally to the standard description of hadronic matter in core collapse supernova studies a phase transition to quark matter. In our scenario, quark matter is composed of up, down and strange quarks. At the conditions where quark matter appears, neutrinos are highly trapped and weak equilibrium is established, i.e. $\mu_d + \mu_{\nu_e} = \mu_u + \mu_e$ and $\mu_s = \mu_d$. For the description of quark matter, we choose the widely used MIT bag model due to its convenient handling. For high densities and temperatures where quark matter occurs, we extend and replace the hadronic EoS table [20] with the corresponding quark matter values. Quarks are described as relativistic fermions, and the confinement of quarks to hadrons below a critical density is expressed through the bag constant B as follows:

$$p_{\text{quark}} = \sum_{i=u,d,s} p_F^i - B, \qquad \epsilon_{\text{quark}} = \sum_{i=u,d,s} \epsilon_F^i + B, \tag{6}$$

where p_F and ϵ_F are the Fermi contributions to the quark pressure and energy density. The simple MIT bag model can be extended by the inclusion of first order corrections in the strong interaction constant α_S. However, in this first approach we focus on the MIT bag model without α_S corrections. Therefore, the critical density for the appearance of quark matter is determined by the bag constant and the strange quark mass $m_s = 100$ MeV. The masses of the up and down quarks are in the range of MeV. Since the baryo-chemical potential of quarks for $\rho > \rho_0$ is of the order $\geqslant$300 MeV, up and down quarks can be treated as massless.

When describing a phase transition from hadronic matter to quark matter, two different approaches are normally chosen. The so-called Maxwell construction assumes local charge neutrality for the quark and hadron phases separately. In contrast, the Gibbs approach allows for electrically different charged phases as long as the total charge of the quark and the hadronic phase is zero. This gives rise to the existence of a mixed phase of quark and hadronic matter between the pure phases. A more general study of phase transitions in the presence of global and local conservation laws was discussed recently in [8]. Finite size effects in the mixed phase, such as surface tension, and Coulomb effects can lead to the appearance of structures, such as spheres, rods or planes of quark and hadronic matter, similar to what is found to happen in the hadronic liquid–gas phase transition [14, 24]. In this work we use the Gibbs construction without finite size effects. The bag constant is chosen to neither conflict with pulsar mass measurements nor with results from heavy ion collisions. The first constraint comes from the up to now highest precisely measured mass, the Hulse–Taylor pulsar with $M_{\text{HT}} = 1.4414 \pm 0.0002$ $\text{M}_\odot$. Therefore, the mass–radius relations of our hybrid star configurations have to fulfil $M_{\text{max}} \geqslant 1.44$ $\text{M}_\odot$. Figure 1(*a*) shows mass–radius curves for different bag constants together with the constraint of the Hulse–Taylor pulsar mass. Either bag constants above $B^{1/4} \sim 190$ MeV or below $B^{1/4} \sim 170$ MeV can reach this limit. However,

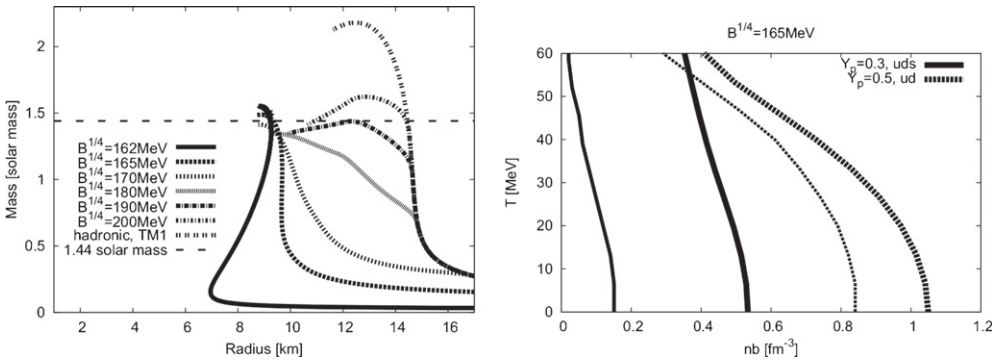

(*a*) Mass-Radius curves. (*b*) Phase diagram.

Figure 1. The limit of the Hulse–Taylor pulsar is given by the horizontal line in graph (a) (mass–radius curves). Only large bag constants and small bag constants with a high and low critical density, respectively, can reach the mass limit of 1.44 $M_\odot$. Graph (b) (the limit of the Hulse–Taylor) compares a phase transition to u,d,s quark matter for supernova environments where $Y_p = 0.3$ and the situation in heavy ion collisions. The lines show the onset (thin) and the endpoint (thick) of the mixed phase. Because matter is isospin symmetric and due to the short timescales, only a phase transition to up and down quark matter is allowed which leads to significantly higher critical densities.

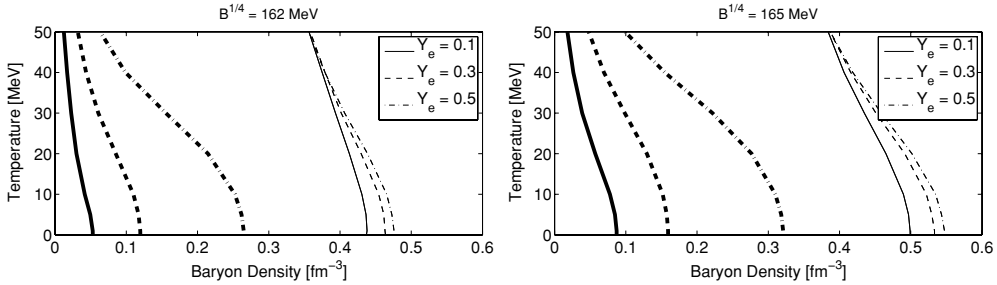

Figure 2. Critical density as a function of the temperature for different asymmetries, for the two quark matter EoSs (left: $B^{1/4} = 162$ MeV, right: $B^{1/4} = 165$ MeV). The lines show the onset (thick) and the endpoint (thin) of the mixed phases.

as mentioned before a bag constant of 200 MeV has already been explored in supernova simulations [16]. We chose the lower values, i.e. $B^{1/4} = 162$ MeV and $B^{1/4} = 165$ MeV. The other criterion is the critical density for the phase transition which should not be in conflict with heavy ion data. Figures 2 show the corresponding phase diagrams for the bag constants chosen in our approach for fixed electron fractions Y_e. The thin lines denote the beginning of the mixed phase, and the thick lines mark the beginning of the pure quark phase. As can be seen for electron fractions of $Y_e \leqslant 0.3$, which are typical for supernova environments, quark matter sets in around saturation density of $n_0 \sim 0.16$ fm^{-3} (in nuclear units).

Such an early phase transition is not in contradiction with heavy ion data since matter in supernova environments is different from the one in colliding nuclei. Matter in heavy ion experiments has a proton fraction of $Y_p \simeq 0.5$, i.e. matter is isospin symmetric or close to isospin symmetry. Furthermore, the expansion timescales in relativistic heavy ion collisions are of the order 10^{-23} s, which are too short to produce strangeness via weak interactions (e.g. $u+d \rightarrow u+s$) where timescales are in the range of 10^{-8} s. In contrast, the supernova dynamics happen on timescales of milliseconds which are long enough to establish weak equilibrium in

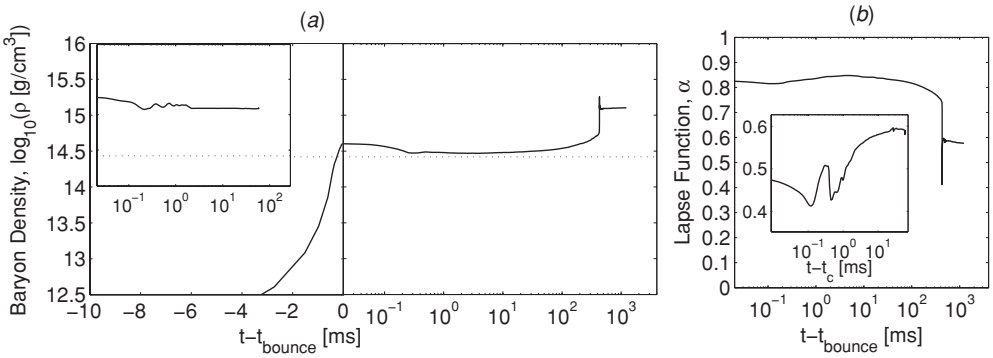

Figure 3. Central density (*a*) and lapse function (*b*) with respect to time after bounce $t_{\rm bounce}$ for the 10 $M_\odot$ progenitor model. The insets show the evolution after the PNS collapse at $t_c = 429.80$ ms after bounce. The time gauges $t_{\rm bounce}$ and t_c are chosen when the maximum central densities are obtained.

the system, especially with respect to $\mu_d = \mu_s$. Figure 1(*b*) shows the behaviour of the critical densities for the two cases. The solid lines represent a phase transition from hadronic matter to up, down and strange quark matter for a proton fraction of $Y_p \simeq 0.3$, and the dashed lines give the phase diagram for heavy ion collisions. Here, the critical densities are higher, around $n \simeq 5 \times n_0$ for the onset of the mixed phase and $n \simeq 1.1$ fm^{-3} for the beginning of the pure quark phase. Figure 1(*b*) illustrates that high critical densities in heavy ion collisions do not exclude a low density onset of quark matter in supernova environments. The inclusion of pions and hyperons in the hadronic EoS for high temperatures and α_s corrections for quark matter can modify the exact location of the critical densities. However, even with these modifications the main statement of the discussed compatibility of quark matter in supernovae and collision experiments will not change.

4. The QCD phase transition during the early post bounce phase

We investigate the quark–hadron phase transition in core collapse supernova simulations in spherical symmetry, where usually no explosion can be obtained. The phase transition happens during the early post bounce accretion period, triggered by the continuously increasing density and temperature and the decreasing electron fraction. The simulations are launched from several Fe-core progenitors in the mass range of 10–15 $M_\odot$ [25].

The evolution of the central density $\rho_{\rm central}$ and lapse function $\alpha_{\rm central}$ are illustrated in figure 3 at the example of the 10 $M_\odot$ progenitor model. $\rho_{\rm central}$ rises during the Fe-core collapse and it exceeds nuclear saturation density ρ_0 (dashed line in figure 3(*a*)) where the core bounces back. Due to the early post bounce expansion, the central density decreases again slightly. However, on a longer timescale of 100 ms during the later mass accretion period, $\rho_{\rm central}$ rises again. It stays strictly above nuclear saturation density, $\rho_{\rm central} > \rho_0$. Additionally, the temperature increases above 10 MeV and the electron fraction decreases to $Y_e \simeq 0.1$–0.2. The central lapse function in figure 3(*b*) decreases during the mass accretion induced PNS contraction continuously to a value of about 0.75. This evolution applies for all massive progenitor stars where normally only hadronic matter is considered.

In the regime of high temperatures and low electron fractions which result from the PNS evolution, quark matter becomes energetically more favourable. The reasons are the large contribution of the symmetry energy to the total energy of isospin asymmetric hadronic matter

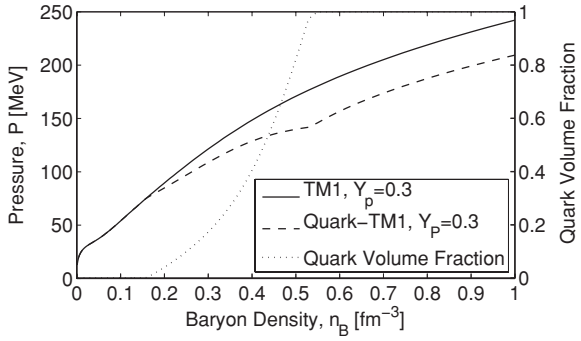

Figure 4. Equations of state for hadronic matter (solid line) and quark matter (dashed line), including the phase transition. The quark fraction (dotted line) is denoted at the right side. The mixed phase sets in around saturation density and softens toward higher densities. Pure quark matter is obtained around $n \simeq 0.5$ fm^{-3}, where the EoS stiffens again significantly.

and the higher number of degrees of freedom in the quark phase. The dynamical evolution of the PNS during the phase transition is illustrated in figure 5. During the post bounce contraction of the PNS, which happens on timescales of 100 ms, hadronic matter is converted into the mixed phase, where the adiabatic index is smaller than in both, the pure quark and the pure hadronic phases. At the beginning of the mixed phase the EoS is similar to the hadronic one, as illustrated in figure 4 at $n_{\rm B} \simeq 0.18$–0.2 fm^{-3}. Therefore, the centre of the PNS first stays in this regime while hadronic matter in the outer regions also enters the mixed phase. Mass accretion onto the surface of the PNS eventually causes an increase in the central density and matter moves to the softer regions of the mixed phase. This, together with the increasing pressure, causes the PNS to become gravitationally unstable and to contract (see velocity profiles in figure 5(*a*) (top panel)). The contraction proceeds into a supersonic adiabatic collapse during which the density increases by about one order of magnitude (see figure 5(*b*) (top panel)). Relativistic effects become important in the presence of the increasing gravitational field obtained due to the compression of the central PNS. The lapse function decreases to $\alpha_{\rm central} \leqslant 0.6$, as shown in figure 5(*c*) (top panel). The higher densities favour the pure quark phase where the adiabatic index increases again, i.e. the EoS stiffens. The collapse halts and a second accretion shock with no matter outflow forms, illustrated via the velocity profiles in figure 5(*a*) (top panel) at about 1.2–1.3 $M_\odot$. This second accretion shock propagates outwards and accelerates to positive velocities at the decreasing density gradient at the phase boundary between the infalling hadronic material and the mixed phase. It detaches from the mixed phase and propagates into the pure hadronic phase, see the velocity and density profiles in figure 5(*a*) and (*b*) (bottom panel) where additional acceleration takes place due to the large density decrease at the PNS surface of several orders of magnitude. Positive velocities of the order 10^5 km s^{-1} are obtained which relates to a highly relativistic matter outflow. The lapse function of the accelerated material decreases significantly from $\simeq$0.95 to 0.6 and the central lapse function stays close to 0.4 after the shock has left the PNS, which has entered a quasi-static state. The second shock finally merges with the SAS from the Fe-core bounce, and an explosion is initiated where otherwise no explosion could be obtained.

During the shock expansion across the neutrinospheres, where neutrinos transfer from the trapped to the free streaming regimes, the lifted degeneracy of the shock-heated hadronic matter adjusts to β-equilibrium at a higher value of the electron fraction. The additionally emitted neutrinos can escape and become observable in the neutrino spectra as an additional

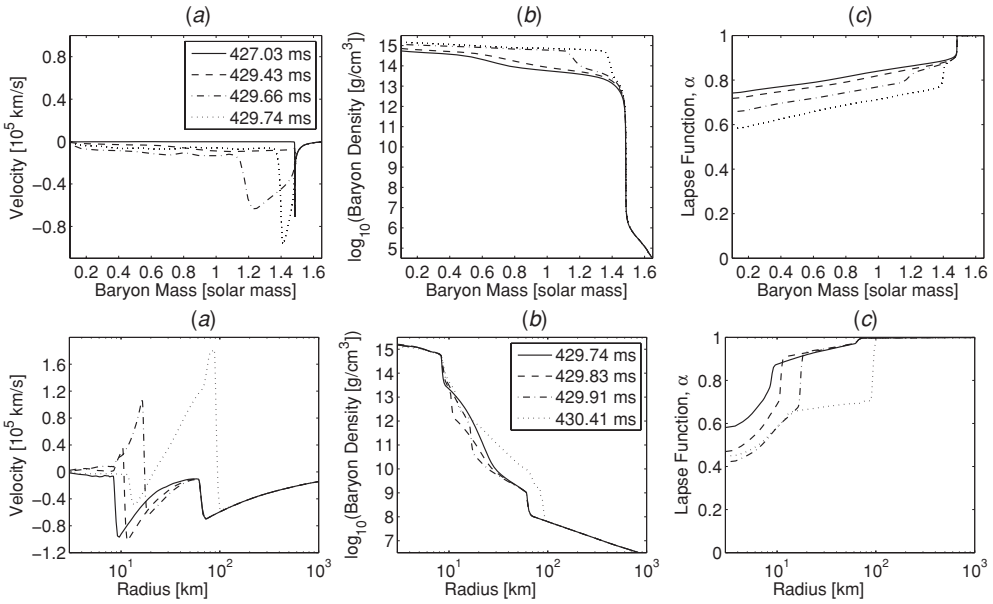

Figure 5. Selected radial variables for different post bounce times, illustrating the PNS collapse (top) and the explosion phase (bottom).

burst, dominated by electron anti-neutrinos due to the increased Y_e as shown in figure 6 for the 10 $M_\odot$ progenitor star. Illustrated is the dynamical evolution of the luminosities and mean neutrino energies with respect to time after bounce, comparing simulations using the quark (thin lines) and hadronic [20] EoSs (thick lines). The small bag constant $B^{1/4} = 162$ MeV in figure 6 (left panel) relates to the lower critical density and hence an earlier onset of the phase transition at about 250 ms post bounce. The delay for the onset of the phase transition in the simulation using the large bag constant $B^{1/4} = 165$ MeV in figure 6 (right panel) is due to a higher critical density and hence a longer accretion time before the critical conditions are obtained at about 420 ms post bounce. The oscillating behaviour of the neutrino spectra after the quark–hadron phase transition is due to the appearance of an additional accretion shock on top of the PNS surface which forms due to neutrino cooling. This additional accretion shock can be identified in the velocity profiles in figure 5(*a*) (bottom) at about 15 km at 430 ms after bounce.

5. Summary and outlook

We performed core collapse simulations of low and intermediate mass Fe-core progenitors in spherical symmetry, where we investigate the appearance of quark matter. Our model is based on general relativistic radiation hydrodynamics and three-flavour Boltzmann neutrino transport. The description of quark matter is based on the MIT bag model where for a given strange quark mass the conditions for the quark–hadron phase transition are fixed by the bag constant and the strange quark mass. Due to the large temperatures of tens of MeV and low electron fractions after core bounce, quark matter appears in form of a quark–hadron mixed phase already close to saturation density. The softening of the EoS for matter in the mixed phase results in an adiabatic collapse. The higher densities and temperatures obtained during the collapse lead to the appearance of quark matter, where due to the stiffening of the EoS a

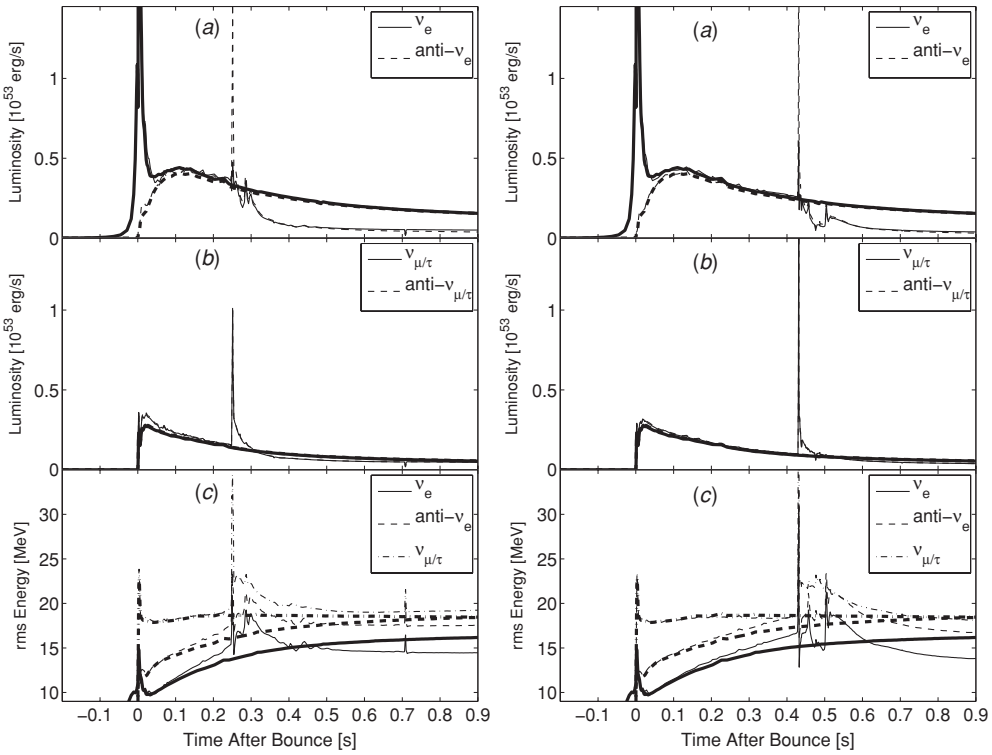

Figure 6. Neutrino luminosities and mean neutrino energies taken in a co-moving reference frame at 500 km, comparing the quark EoSs (thin lines) with $B^{1/4} = 162$ MeV (left panel) and $B^{1/4} = 165$ MeV (right panel) with the pure hadronic EoS (thick lines) for the 10 $M_\odot$ progenitor model.

strong second shock wave forms. The second shock accelerates to positive velocities of the order of the vacuum speed of light, which launches an explosion where otherwise no explosion could be obtained. In other words a new explosion mechanism of massive stars was found, which works even for spherically symmetric models, where general relativistic effects are important in the presence of strong gravitational fields and relativistic velocities.

The subsequent propagation of the shock across the neutrinospheres releases an additional burst of neutrinos, dominated by electron anti-neutrinos due to the lifted degeneracy of the shock-heated hadronic matter. The magnitude and delay of the second neutrino burst contain correlated information about the PNS evolution, which is given by the progenitor and the EoS. The millisecond features in the neutrino spectra observed may be resolvable by present neutrino detectors such as IceCube and Super-Kamiokande for a galactic event if quark matter appears, where neutrino oscillations may have a non-negligible effect on the neutrino spectra observed. However, the inclusion of neutrino oscillations is beyond the scope of the present work. Their influence as well as the possible detectability of the neutrino signal from the quark–hadron phase transition is investigated in [5].

The neutrino burst provides an indirect identification of the QCD phase transition since the conditions relate to the regime where neutrinos are highly trapped. On the other hand, gravitational waves may provide a direct probe of the QCD phase transition. In order to predict the gravitational wave spectra emitted from the QCD phase transition in core collapse supernova simulations, a detailed study in multiple spatial dimensions including sophisticated input physics is required.

The ability to identify the QCD phase transition in the observable neutrino or gravitational wave spectra from a future galactic event might allow to constrain the EoS of strongly interacting matter from astronomical observations.

Due to the lifted degeneracy during the shock propagation through the previously shock-heated hadronic matter, the second peak in the neutrino spectra associated with the quark–hadron phase transition is dominated by electron anti-neutrinos. It additionally indicates that a reasonable amount of neutron-rich matter is ejected on a fast expansion timescale. Both conditions may favour the production of heavy elements via the *r*-process, which has to be confirmed via detailed *r*-process nucleosynthesis calculations.

Acknowledgments

The project was funded by the Swiss National Science Foundation grant no PP00P2-124879/1 and 200020-122287 and the Helmholtz Research School for Quark Matter Studies, the Italian National Institute for Nuclear Physics, the Graduate Program for Hadron and Ion Research (PG-HIR), the Alliance Program of the Helmholtz Association (HA216/EMMI) and the DFG through the Heidelberg Graduate School of Fundamental Physics. The authors are additionally supported by CompStar, a research networking program of the European Science Foundation, and the Scopes project funded by the Swiss National Science Foundation grant no IB7320-110996/1. A Mezzacappa is supported at the Oak Ridge National Laboratory, which is managed by UT-Battelle, LLC for the U.S. Department of Energy under contract DE-AC05-00OR22725.

References

[1] Bethe H A and Wilson J R 1985 *Astrophys. J.* **295** 14
[2] Bionta R M, Blewitt G, Bratton C B, Caspere D and Ciocio A 1987 *Phys. Rev. Lett.* **58** 1494
[3] Bruenn S W 1985 *Astrophys. J. Suppl. Ser.* **58** 771
[4] Burrows A, Hayes J and Fryxell B A 1995 *Astrophys. J.* **450** 830
[5] Dasgupta B, Fischer T, Horiuchi S, Liebendörfer M, Mirizzi A, Sagert I and Schaffner-Bielich J 2009 *Phys. Rev. Lett.* (submitted) (arXiv:astro-ph/0912.2568 [astro-ph.HE])
[6] Fischer T, Whitehouse S C, Mezzacappa A, Thielemann F-K and Liebendörfer M 2009 *Astron. Astrophys.* (submitted) (arXiv:astro-ph/0908.1871 [astro-ph.HE])
[7] Gentile N A, Aufderheide M B, Mathews G J, Swesty F D and Fuller G M 1993 *Astrophys. J.* **414** 701
[8] Hempel M, Pagliara G and Schaffner-Bielich J 2009 arXiv:astro-ph/0907.2680
[9] Herant M, Benz W, Hix W R, Fryer C L and Colgate S A 1994 *Astrophys. J.* **435** 339
[10] Hirata K S *et al* 1988 *Phys. Rev.* D **38** 448
[11] Janka H-Th and Müller E 1996 *Astron. Astrophys.* **306** 167
[12] Kitaura F S, Janka H-Th and Hillebrandt W 2006 *Astron. Astrophys.* **450** 345
[13] Liebendörfer M, Messer O E B, Mezzacappa A, Bruenn S W, Cardall C Y and Thielemann F-K 2004 *Astrophys. J. Suppl. Ser.* **150** 263
[14] Maruyama T, Chiba S, Schulze H-J and Tatsumi T 2008 *Phys. Lett.* B **659** 192
[15] Miller D S, Wilson J R and Mayle R W 1993 *Astrophys. J.* **415** 278
[16] Nakazato K, Sumiyoshi K and Yamada S 2008 *Phys. Rev.* D **77** 103006
[17] Nomoto K 1983 *Supernova Remnants and their X-ray Emission* (*IAU Symposium* vol 101) pp 139
[18] Nomoto K 1994 *Astrophys. J.* **277** 791
[19] Nomoto K 1987 *Astrophys. J.* **322** 206
[20] Shen H, Toki H, Oyamatsu K and Sumiyoshi K 1998 *Nucl. Phys.* A **637** 435
[21] Takahara M and Sato K 1988 *Prog. Theor. Phys.* **80** 861
[22] Thielemann F-K, Brachwitz F, Höflich P, Martínez-Pinedo G and Nomoto K 2004 *New Astron. Rev.* **48** 605
[23] Timmes F X and Arnett D 1999 *Astrophys. J. Suppl. Ser.* **125** 277
[24] Voskresensky D 2002 *Phys. Lett.* B **541** 93
[25] Woosley S E, Heger A and Weaver T A 2002 *Rev. Mod. Phys.* **74** 1015